Combustion Behaviours of Iron Particles in Varied Atmospheres

Paul Picotte

Supervised by Professor Jeffrey Bergthorson

A Thesis submitted to McGill University in partial fulfilment
of the requirements of the Undergraduate Honours Program.

Department of Mechanical Engineering, McGill University

817 Sherbrooke Street West, Montreal, QC, H3A 0C3

April 14th, 2020

Abstract

The combustion characteristics of iron particles in different oxidizing mixtures was observed experimentally and compared against two theoretical combustion models. Combustion atmospheres were varied to observe the influence of the transport properties of the oxidizing gas and oxygen concentration on the combustion characteristics of a single iron particle, 16-microns in diameter. A drop tube furnace apparatus was built to allow filming of the combustion events with the use of a high-speed camera, while introducing various gas mixtures into the experimental section of the furnace. The results showed the time-dependent combustion model to be more accurate in predicting combustion times as it accounted for the dynamic transitions between the combustion regimes, whereas the regime-dependent models did not. Further, combustion in the helium-oxygen gas mixtures was observed to be burning in a more kinetically-limited regime than the argon-oxygen mixture. Increasing the oxygen concentration was experimentally observed and theoretically shown to increase the combustion's brightness and temperature while decreasing the combustion time.

NOTE: The full scope of the intended research was not completed due to the restrictions imposed by the COVID-19 pandemic. Specific details are mentioned throughout the document, where applicable.

Abrégé

Les caractéristiques de combustion des poudres de fer dans différents mélanges oxydants ont été observées expérimentalement et comparées à deux modèles théoriques de combustion. Les atmosphères de combustion ont été variées pour observer l'influence des propriétés de transport du gaz oxydant et de la concentration en oxygène sur les caractéristiques de combustion d'une seule particule de fer de 16 microns de diamètre. Un appareil de fourneau à tube vertical a été construit pour permettre le tournage des événements de combustion à l'aide d'une caméra à haute vitesse, tout en introduisant divers mélanges de gaz dans la section expérimentale de l'appareil. Les résultats ont montré que le modèle de combustion dépendant du temps était plus précis dans la prévision des temps de combustion car il prend en considération les transitions dynamiques entre les régimes de combustion, contrairement aux modèles dépendant du régime. En outre, la combustion dans les mélanges hélium-oxygène a été observée comme étant plus limitée cinétiquement que le mélange d'argon-oxygène. Une augmentation de la concentration en oxygène a été expérimentalement observée et théoriquement montrée d'augmenter la luminosité et la température de la combustion tout en diminuant le temps de combustion.

REMARQUE: La portée entière de la recherche prévue n'a pas été achevée en raison des restrictions imposées par la pandémie COVID-19. Des détails spécifiques sont mentionnés dans tout le document, le cas échéant.

Acknowledgements

I would like to thank to my thesis supervisor, Jeffery Berthorson, for his guidance and support throughout my thesis. I would also like to thank the entire Alternative Fuels Laboratory, for sharing valuable insights and their inspiring passion for renewable alternatives to fossil fuels. I am particularly grateful to Jan Palečka for his many explanations, demonstrations, and overall introduction to academic research.

Table of Contents

List of Tables

List of Figures

1. Introduction

1.1 Context

The contemporary global development of countries has seen increases in the demand for cheap and reliable energy to enable their transformations. In the past two centuries, this demand has been almost entirely provided by fossil fuels, as shown in Figure 1.

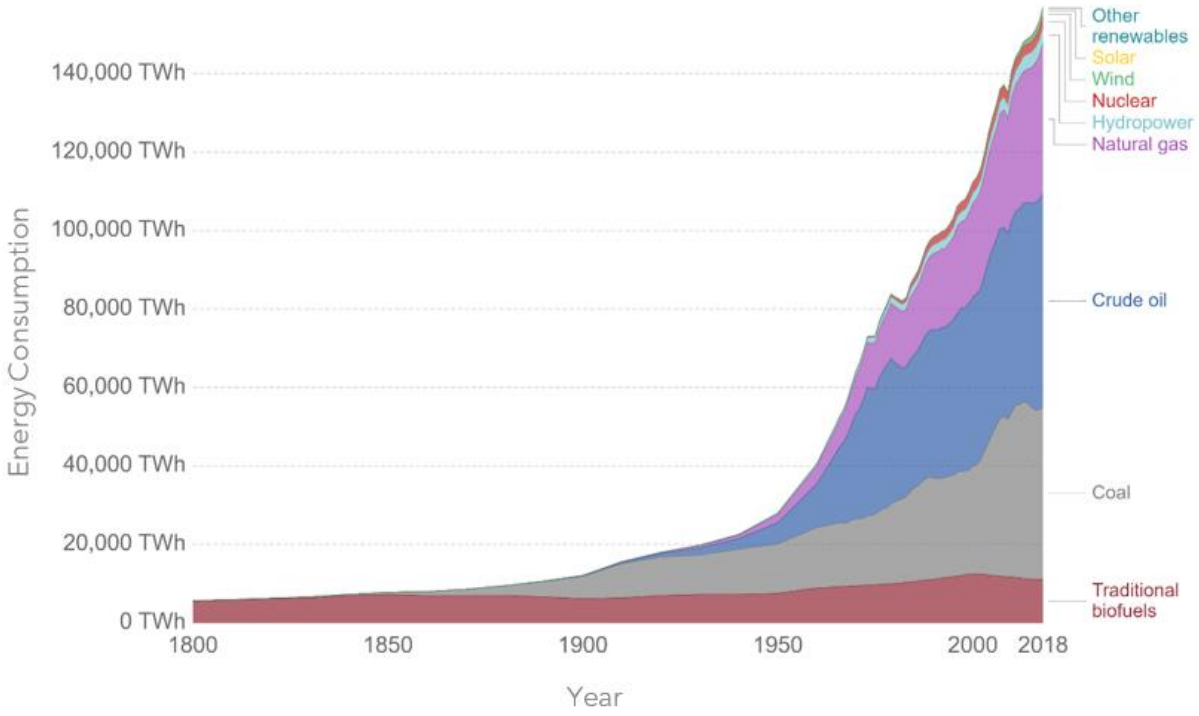

Figure 1: Global primary energy consumption by year[1, 2].

This can be largely attributed to the many attractive properties of fossil fuels: high energy and power densities, relatively low costs, readily available worldwide, and easily transportable. However, their use presents two main problems. First, the emission of carbon dioxide as a product of its combustion is associated with global warming, whose complex set of consequences have

increasingly negative ecological, sociological, and economic impacts. Second, the resources are non-renewable and will therefore be increasingly more expensive to extract as the sources of fossil fuels become more remote or unconventional[3-5].

This dilemma has spurred a search for alternatives solutions to replace fossil fuels. Many proven solutions already exist to replace fossil fuel-powered power plants such as hydro, solar, wind, nuclear, and geothermal energies. However, matching the energy-density and convenience of fossil fuels with a different energy carrier capable of similar performance proves to be a more challenging problem. Mechanical and chemical energy storage are both mature technologies, but have small energy densities and specific energies compared to fossil fuels, as shown in Figure 2.

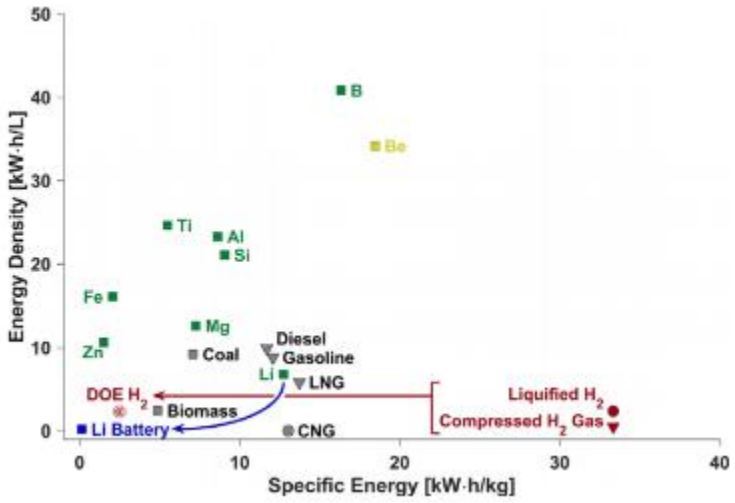

Figure 2:Comparison of energy density and specific energy between metal fuels, hydrocarbons, and batteries [4].

Metal fuels show promise as energy carriers due to their high energy density and their ability to carry energy by completing a metal redox cycle. This would have the potential to be a near zero-

carbon loop if the reduction of the oxide is done with the use of a low-carbon energy source. Furthermore, metals are abundantly available in the earth's crust.

1.2 Motivation

The Alternative Fuels Laboratory at McGill University is proposing the dry cycle, where metal fuel is directly reacted in air. Iron is a primary candidate fuel as it has a moderate adiabatic flame temperature (2230 K in air), which is below the boiling point of the metal (3130 K) and experiences heterogenous combustion occurring on the surface of the particle thus facilitating theoretical modelling of the combustion[6]. It also has a well-established method of recycling through the reduction of iron oxide back into iron power and is an abundant resource on earth[4, 7].

To that end, this thesis will help to develop the understanding of iron combustion to support and inform the development of dry cycle systems using iron as the metal fuel. Specifically, by investigating the influence of atmospheres on the characteristics of combustion. The goal of this thesis is also to develop data which could later serve to determine the optimal operating points to maximise the effectiveness of combustion while imposing realistic conditions for the development of dry cycles using iron as a metal fuel. Further, this thesis will compare the experimental data with the various theoretical models for the combustion mechanics of single particles. Due to the COVID-19 outbreak, only one particle size was tested.

1.3 Outline

The subsequent chapters of this thesis are organized as such:

Chapter 2 covers the theoretical background of this research, mainly discussing the theory of metal particle combustion.

Chapter 3 presents the design of the experiment. Specifically, discussing the particle and gas mixtures, design of the testing apparatus, and analysis method.

Chapter 4 presents and analyses the experimental data, divided by gas mixtures, and the result of the theoretical models. A discussion on the sources of error is included in the last section of the chapter.

Chapter 5 discusses the observed trends in the data presented in chapter 4.

Chapter 6 concludes by summarizing the key findings of the experiment and proposes future areas of work for this experiment.

2. Theoretical Background

2.1 Single Metal Particle Combustion

2.1.1 Single Iron Particle Combustion Modes

To better understand the choice of iron particles for use as a metal fuel, a background in single iron particle combustion is briefly explained.

Whereas combustion of gaseous fuels and oxidisers allow for premixing at the molecular level prior to combustion, metal particles can only be premixed to the extent of the size of the particles. As a result, gaseous fuel-oxidizer mixtures burn mostly homogeneously at a rate dictated by the chemical kinetics of the reactants, whereas metal particles burn in two different modes: either heterogeneously, with the reaction occurring on the particle's surface, or in diffusion micro-flames surrounding the particle.

The dichotomy in metal combustion modes is determined by the metal oxide's volatilization temperature relative the boiling point of the metal fuel. For a metal fuel to burn in the gaseous phase, the heat of the surrounding gas must be greater than the metal's boiling point. This condition requires the oxide's volatilization or vaporization-dissociation temperature to be greater than the than the metal's boiling point to sustain the metal fuel's evaporation as illustrated in Figure 3 A. This concept, known as "Glassman's criterion", states that for non-volatile metals, the maximum flame temperature is limited by the resulting oxide's volatilization point and that metals will burn heterogeneously if the oxide vaporization-dissociation temperature is below its boiling point. [3, 8, 9]. In heterogenous combustion, the metal oxides will either be gaseous and diffuse away from

the particle, or oxides will form and encase the metal particle, as shown in Figure 3 B and C respectively.

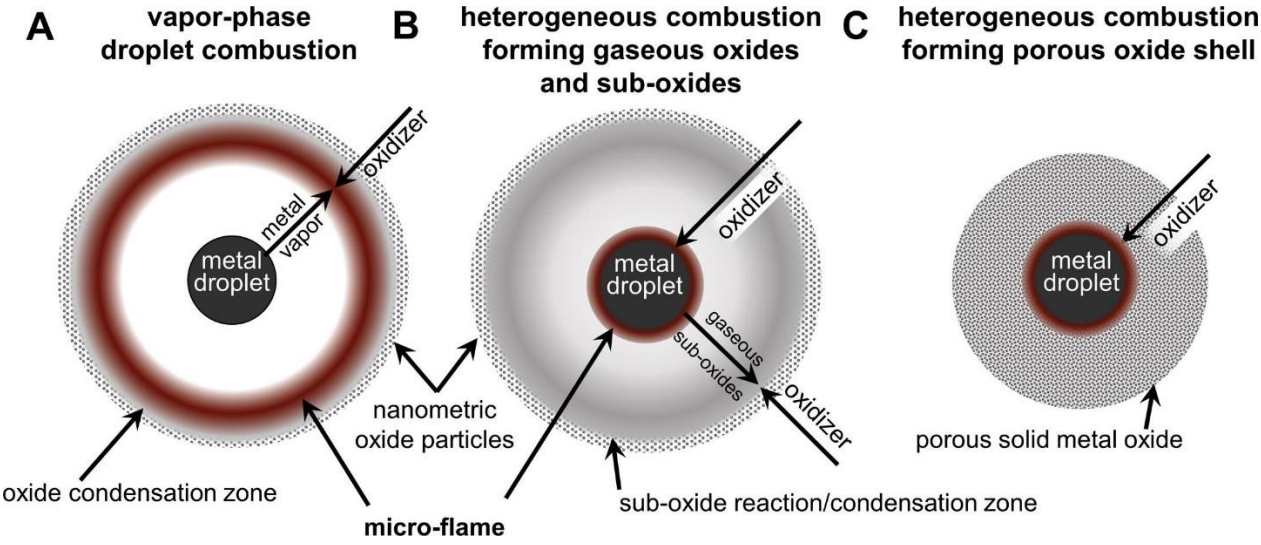

Figure 3: Volatile and non-volatile particle combustion modes [3].

Using a thermodynamic equilibrium solver, Iron was determined to have an adiabatic flame temperature of 2230 K in air and a boiling point of 3130 K. It was also determined that iron produces condensed-phase products Fe_3O_4 (83%) and FeO (17%) in air, and has a negligible partial pressure of gaseous oxides [3, 6]. Since Iron's flame temperature is below its boiling point and the volatilization point of its oxides, the particle combustion is very heterogenous[10, 11]. Further, the low flame temperature implies that none of the oxides can be in the gaseous form and so the combustion is predicted to form a porous oxide shell around the iron particle, as illustrated in Figure 3, case C.

Therefore, iron is an ideal candidate for the purposes detailed in the motivation section of this thesis. Specifically, iron has the unique property of not creating vapour-phase oxides, making recuperation of its oxides in the exhaust for recycling a possibility.

2.1.2 Modeling the rate of heterogenous reactions

To describe the rate of iron combustion, a model initially developed by Frank-Kamenetskii and Vulis is employed. The model uses a quasi-steady state approximation to determine the heterogenous reaction rate for spherical particles. The approach assumes that the surface reaction rate follows a single-step first-order Arrhenius reaction:

$$k = k_0 exp\left(\frac{-E_a}{RT_s}\right) \quad (1)$$

Where k_0 is a pre-exponential factor, E_a is the activation energy, R is the universal gas constant, and T_s is the temperature of the particle, which is equivalent to the surface temperature since the particles are assumed to have small Biot numbers and thus have negligible internal temperature distribution. Oxidizer consumption on the particle surface is given by:

$$\frac{dm}{dt} = C_s A k \quad (2)$$

Where C_s is the concentration of oxidiser at the particle surface, k is the kinetic rate, determined in equation **Error! Reference source not found.**(1) and A is the particle surface area, $4\pi r^2$.

The mass-transfer coefficient between the gas and particle per surface area is given by:

$$\beta = \frac{DSh}{L} = \frac{D}{r_p} \quad (3)$$

Here, D is the mass-diffusivity of the oxidizer and r_p is the particle radius. Equation (3) assumes Sh=2 , because the particle is assumed to be spherical and with no velocity slip, and that the Stefan flow, caused by the movement of mass and heat around the particle, is negligible. This is since the effects of Stefan flow are small when the number of moles of consumed oxidiser is approximately equal to the number of moles of reaction products or when the partial pressure of the oxidizer is much less than unity [8, 12].

By assuming quasi-static equilibrium, the oxidiser concentration at the particle surface is dictated by the difference between the rate of oxidizer transport and consumption as shown.

$$AC_s k = A\beta(C_0 - C_s) \rightarrow C_s = C_0\left(\frac{\beta}{k+\beta}\right) \tag{4}$$

Where C_0 is the oxidizer concentration in the free stream, and C_s is the oxidizer concentration at the particle surface.

By substituting equation (4) into equation (2), an expression accounting for diffusion of oxides and reaction kinetics is obtained:

$$\frac{dm}{dt} = C_0 A\beta\left(\frac{k}{k+\beta}\right) \tag{5}$$

The reaction rate, determined by the rate of consumption of oxidizer in equation (5), shows a dependence on the both the kinetic, $k(T_s)$, and diffusive, $\beta(\mathrm{r_p})$, terms of the reaction.

To express the interaction between the combustion regimes, a normalized Damköhler number,

$$Da^* = \frac{Da}{1+Da} = \frac{k}{k+\beta} \tag{6}$$

can be used, where the Damköhler number, Da = k/β. Equation (5) can thus be rewritten:

$$\frac{dm}{dt} = C_0 A \beta Da^* \tag{7}$$

When the combustion reaction is in the kinetically limited regime, $\beta \gg k$ and so Da^* approaches 0. In the diffusively limited regime, $\beta \ll k$ so Da^* approaches unity [12]. The physical implications of the two different regimes are made evident by observing the behaviour of equation (7). In the kinetic regime, the equation approaches $\frac{dm}{dt} = C_0 A k$ indicating that the rate of consumption of oxidizer is determined by the kinetics, and that the concentration at the particle surface C_s is close to the bulk gas concentration C_0, from equation (4). Contrarily, in the diffusive regime, equation (7) approaches $\frac{dm}{dt} = C_0 A \beta$, showing that the rate of reaction is exclusively dependent on the diffusive term. Further, the concentration at the particle surface C_s approaches 0 since the kinetic term in equation (4) is so dominant. These characteristics are depicted in Figure 4.

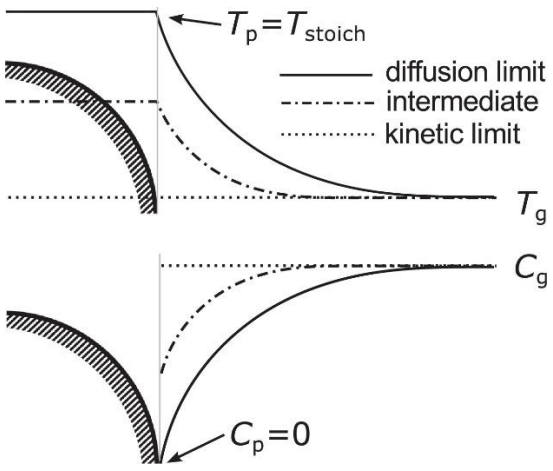

Figure 4: Temperature and oxidizer profiles for particles burning in the kinetic and diffusive regimes[8].

In the kinetic regime the particle burns at a rate exponentially dependent on temperature, has a surface temperature close in value to the local gas temperature, and oxidiser concentration levels is nearly that of the surrounding gas [13, 14]. Contrarily, the diffusive regime has oxidiser concentrations approaching 0 at the surface, while the temperature approaches the adiabatic flame temperature. The relationship between the combustion regimes and surface temperature are further explained in section 2.1.5.

2.1.3 Regime-Dependent Combustion Time Model

The experimental results collected in this thesis are compared against two theoretical models. The first is the regime dependent combustion time model, which takes two forms depending on the combustion regime of the reaction:

In the kinetically limited regime, the burn time is linearly proportional to the diameter of the particle,

$$t_{b,kin} = \frac{\rho_p d_0}{2i\rho m_{0.\infty} k} \tag{8}$$

where ρ_p is the particle density, d_0 is the particle diameter, i is the mass stoichiometric ratio, and $m_{0,\infty}$ is the mass fraction of oxygen and k is the kinetic rate constant, shown in equation (1)[7, 14].

In the diffusive regime, the burn time is proportional to the square of the particle diameter,

$$t_{b,diff} = \frac{\rho_p d_0^2}{8\rho D ln\left(1 + i m_{0,\infty}\right)} \tag{9}$$

Where D is the diffusivity of the gas, and ρ is the gas density [7].

This theoretical model is valid for particles at the diffusion or kinetic limits. In reality, the particle size constantly changes as the combustion proceed. Therefore, using a time-dependent combustion model may give a more accurate understanding of combustion occurring between the two regimes.

2.1.4 Time-Dependent Combustion Analysis

By considering the changes in particle mass throughout the combustion event, it can be shown that particles may transition between regimes, causing the particle temperature to change accordingly. The transition from the kinetic to diffusive regime, known as ignition, occurs when the rate of the particle heat generation, $\dot{Q}_R$, starts exceeds the rate of particle heat loss, $\dot{Q}_L$.

Recalling equation (5), the rate of heat generation is given by,

$$\dot{Q_R} = qi\frac{dm}{dt} = qiA\beta\frac{k}{k+\beta}C_0 \tag{10}$$

Where q is the heat of reaction per unit mass of the reaction, i is the stoichiometric ratio of fuel to oxidiser, C_0 is the surrounding gas oxidiser concentration, and A is the particle surface area.

Assuming radiative heat transfer is negligible, the rate of heat loss is expressed as

$$\dot{Q_L} = hA(T_s - T_0) \tag{11}$$

where A is the surface area, T_s and T_g are the surface and gas temperatures, and h is the convective heat transfer coefficient, given by

$$h = \frac{Nu\lambda}{2r_p} = \frac{\lambda}{r_p} \tag{12}$$

where Nu = 2 for a spherical particle with no velocity slip. In equation (12), λ is the gas thermal conductivity and r_p is the particle radius.

As the mass of the particle is consumed in the reaction and the radius shrinks, the rate of heat generation falls more quickly than the rate of rate of heat loss. This relationship is qualitatively shown in Figure 5, where a particle of size r_2 ignites upon reaching the ignition temperature T_{g0}, transitioning to the diffusive regime. The particle then loses mass to the chemical reaction, causing the radius to approach r_1 and the heat loss line to become steeper relative the heat generation line, eventually resulting in extinction as the particle size falls below r_1.

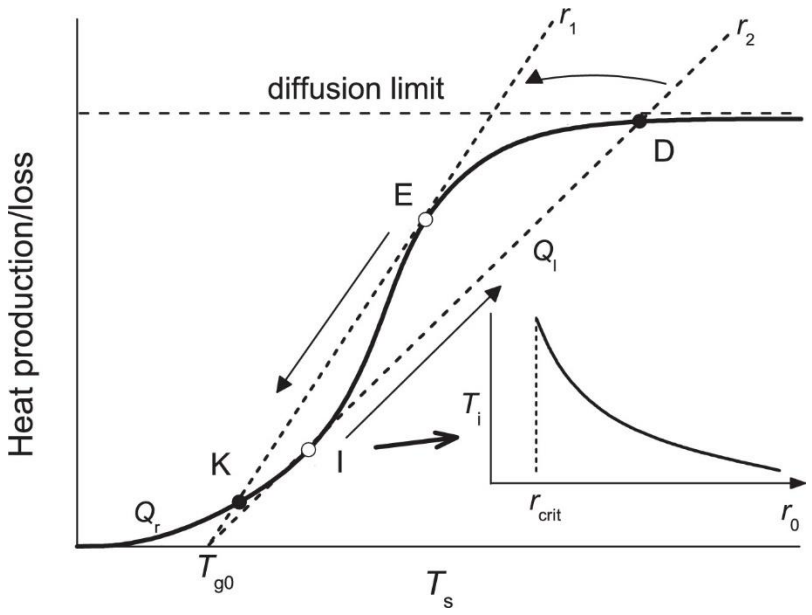

Figure 5: Semenov diagram showing ignition at particle size r_2 and extinction at particle size r_1 [12]

To examine the change in the reaction regimes over time, the time-dependent combustion energy expression is given as,

$$c_s \frac{d(mT_s)}{dt} = \dot{Q}_R - \dot{Q}_L = qiA\beta \frac{k}{k+\beta} C_0 - hA(T_s - T_0) \tag{13}$$

and the rate of change of particle mass is simply the negative of the rate of consumption of the fuel:

$$\frac{dm}{dt} = -\mathrm{iA}\beta \frac{k}{k+\beta} C_0 \tag{14}$$

Equations (13) and (14) form a set of ordinary differential equations governing the dynamics of a single particle burning heterogeneously. The equations were integrated using MATLAB in [8], resulting in Figure 6, showing the particle temperature and mass profiles, as well as the normalized Damköhler number to understand the dominance of combustion regimes.

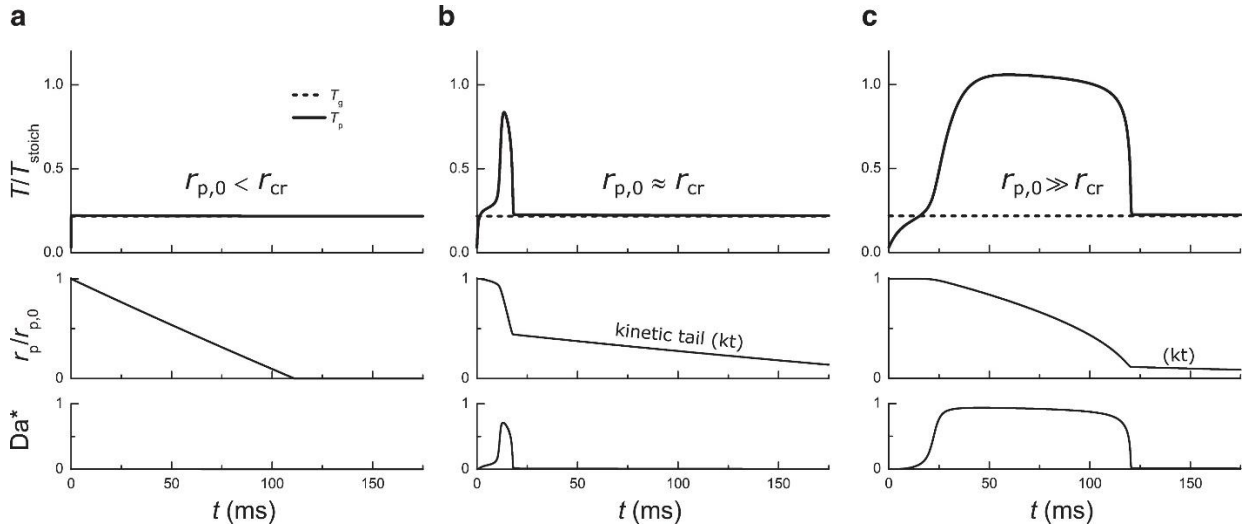

Figure 6: Temperature, radius, and normalized Damköhler over time for three particle sizes

In case a) of Figure 6, the initial particle size is below the critical radius: the value below which the heat loss rate exceed the heat generation rate for any particle temperature [13]. Therefore, the particle cannot ignite and burns entirely in the kinetic regime, the particle radius decreases linearly, and Da^* is close to 0.

In case b), the particle is initially slightly above the critical radius and thus ignites and experiences a sharp increase in temperature until the radius is sufficiently reduced such that extinction occurs and the combustion continues in the kinetic regime. The particle mass is consumed in both the initial diffusive regime and subsequent kinetic regime making the burn time a function of both regimes. Correspondingly, the Da^* number shows a spike towards unity, indicating a more diffusive-controlled rate of reaction for a moment, before dropping back towards 0.

Case c) shows a much larger particle ignite and maintain a temperature close to the adiabatic flame temperature, while the Da^* number is close to 1, both showing that the combustion is strongly in the diffusive regime initially. The Da^* number and temperature proceed to quickly drop, returning to the kinetic regime, after most of the particle mass has been consumed.

These results and theory are critical in qualitatively understanding the behaviours of particles in a mixed combustion regime and is used to explain experimental observations in chapter 4.

2.1.5 Effect of Atmosphere on Flame Temperature

By combining and rearranging equations (10), (11), and (6), the relationship between the combustion regime and temperature can be shown:

$$T_s - T_0 = \frac{D}{\lambda}\left(\frac{k}{k+\beta}\right) qiC_g \; = \; \frac{D}{\lambda}(\mathrm{Da}^*) qiC_g \qquad (15)$$

As discussed in section 2.3, when the reaction is kinetically limited, Da^* approaches 0 and so the difference between the particle surface temperature and the surrounding gas temperature also approach 0. When the reaction is diffusively limited, Da^*approaches 1. Assuming a Lewis number of unity, $Le \; = \; \alpha/\mathrm{D} \; = \; 1$, equation (15) can be rewritten as,

$$T_s = T_0 + \frac{D}{\alpha}(\mathrm{Da}^*)\frac{qiC_0}{c_0\rho_0} = T_0 + \frac{qiC_0}{c_0\rho_0} = T_{stoich} \quad (16)$$

where ρ_0 and c_0 are the gas density and heat capacity, showing that particle temperature in the diffusive regime approaches the stoichiometric flame temperature, explaining the trends seen in Figure 4 and Figure 6 [8].

If the particles burn in the diffusive regime, equation (16) shows that increasing oxidizer concentration, C_0, increases T_{stoich} while increasing c_0 and ρ_0 will lower T_{stoich}. Intuitively, a larger concentration of oxygen would mean increasing the frequency of oxygen colliding with the particle surface. Further, it would also reduce the fraction of non-reactant gases which absorb heat while not contributing to the oxidizing reaction.

2.2 Stokes' Law and Terminal Velocity

This theoretical section serves to better understand the dynamics of micron-sized particles through air as is the case in the experiment. The dominance of viscous forces in considering motion of a micron-sized particles moving through air can be seen by inspecting the Reynold's number:

$$Re = \frac{\rho u D}{\mu} \quad (17)$$

where ρ is particle density, u is the particle velocity, μ is the dynamic viscosity, and D is the particle diameter. In micron-sized particles, the numerator, representing the inertial term, becomes very small causing the expression to be dominated by the viscous term. This means that for such particles, the terminal velocity of occurs when the frictional and buoyant forces acting on the particle is equal to the force of gravity exerted on the particle. Stokes' derivations in [15] result in

an expression for the terminal velocity of a small, sphere moving through a fluid, now known as Stokes' Law:

$$v = \frac{2}{9}\frac{\rho_p - \rho_f}{\mu} g R^2 \tag{18}$$

Where g is the gravitational field strength, R is the radius of spherical particle, ρ_p is density of the particle, ρ_f is density of the fluid, and μ is the dynamic viscosity.

2.3 Particle Heating

The particles used in this experiment are extremely small and thus the Biot number for a sphere,

$$Bi = \frac{hr}{3k} \tag{19}$$

is << 0.1 since the radius, r, is around six orders of magnitude smaller than the other parameters. Therefore, the use of a lumped capacitance analysis to determine the heat of the particle over time is justified. This is expressed as:

$$\frac{T(t) - T_\infty}{T_i - T_\infty} = e^{-Bi*\frac{\alpha t}{L_c^2}} \quad where \quad \alpha = \frac{k}{\rho c_p} \tag{20}$$

where T(t) is the temperature of the particle at a given time, T_i is the initial temperature, T_∞ is the surrounding temperature, r is the particle radius, ρ and C_p are the particle density and heat capacities of iron.

3. Experimental Design

Unfortunately, due to the COVID-19 pandemic, not all planned experiments were conducted as access to the laboratory was restricted. Nonetheless, the variables that were tested and the experimental apparatus and method used are discussed in this chapter.

3.1 Iron Powders and Oxidizers

Only one iron powder size was tested before the laboratory was closed off. The size distribution was determined using a HORIBA LA-920 particle size analyser. The mean particle size is 16.28 microns as shown in Figure 7.

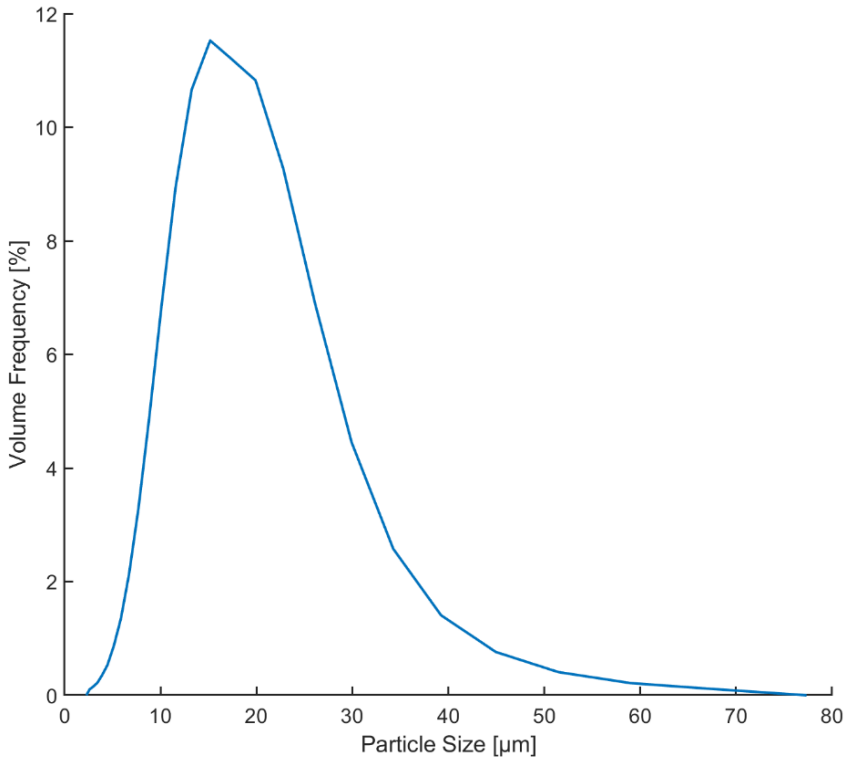

Figure 7: Particle size distribution

The gas mixtures used were:

- Argon (79%) Oxygen (21%)
- Argon (60%) Oxygen (40%)
- Helium (79%) Oxygen (21%)
- Helium (60%) Oxygen (40%)
- Nitrogen (79%) Oxygen (21%) – Air

Unfortunately, tests with Xenon were not conducted before the laboratory closure.

3.2 Drop Tube Furnace

To observe the combustion characteristics of the iron power in different atmospheres, a tubular drop furnace was built to allow iron particles to be dropped using a syringe needle into a quartz tube containing a heated gas. Bleeding flows of the various gas mixtures were introduced from the bottom of the tube. The combustion events were filmed through the opening in the semi-cylindrical heater using a Photron SA1 high-speed camera equipped with macro lenses. A rendering of the experimental setup is shown in Figure 8.

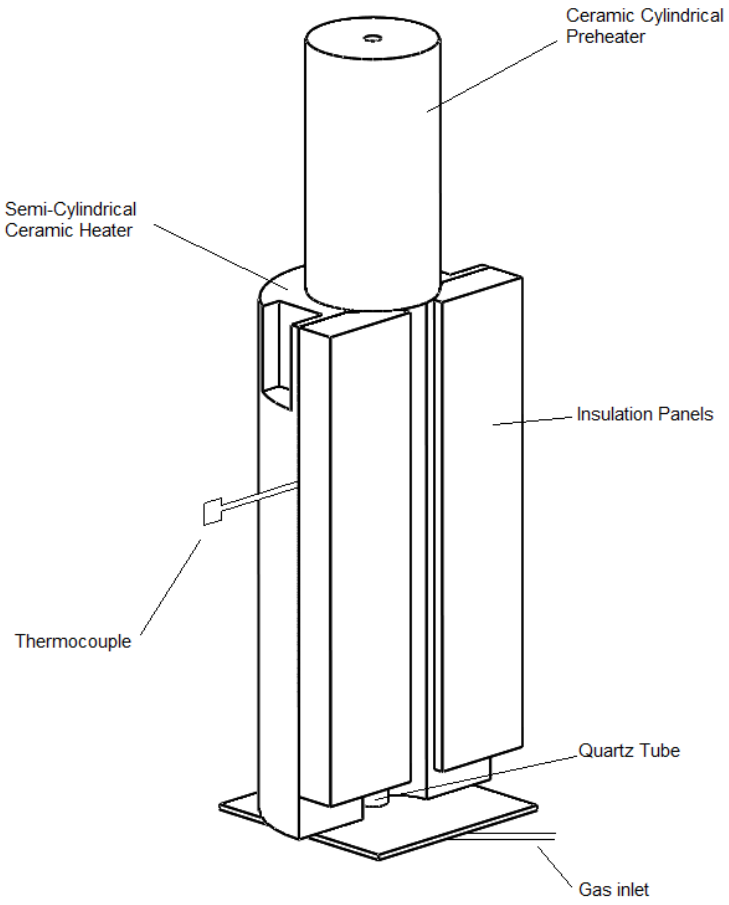

Figure 8: Experimental setup. Particles are injected using a syringe at the top of the cylindrical preheater

The preheater temperature can be modified such that particles enter the experimental section at a temperature around 750K to minimize the particle heating time and ensure that particles combust at a predictable location for easier recording.

To determine the preheater temperature, particles were assumed to be falling at their terminal velocity, given by equation (18), from which the time the particle falls through the preheater can be calculated. By rearranging equation (20), the exit temperature can be obtained as a function of the preheater temperature, expressed as T_∞ in the equation. Since only one particle size was used

due to the COVID-19 outbreak, a preheater temperature of 750K (475 °C) was maintained for all the experiments.

3.3 Optical Conditions and Image Processing– MATLAB Program

The videos collected by the high-speed camera were processed using a MATLAB program. By splitting the videos into their frames, and binarizing each frame, the contour, area, and light intensity of each particle at each frame could be recorded and subsequently plotted against time. Figure 9 shows the program correctly identifying particles between frames by tracing their centroids over time.

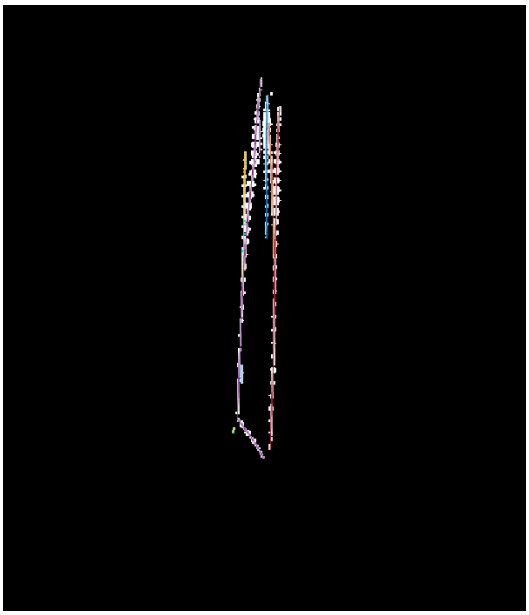

Figure 9: Multiple frames superimposed to show particle-tracking results of MATLAB program

In order to prevent saturation, the aperture on the lens and optical filters used had to be varied for each atmosphere since the intensity of the combustion changes depending on the composition of oxidizing gas. However, despite the changes in optical conditions, most graphs plotting light intensity against time were still oversaturated. In other words, the pixel value reached its maximum

value for the majority of the plot. Instead, to obtain the combustion characteristics of the particles, the area of bright spots was plotted against time. This observation is shown in Figure 10.

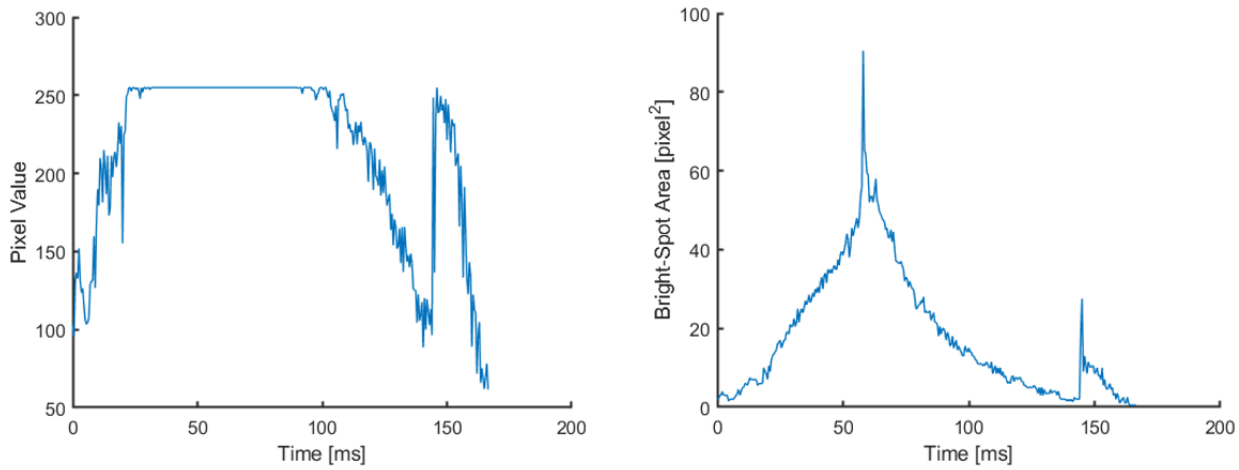

Figure 10: Left, light intensity of a particle vs. time, note the saturation at the maximum pixel value of 255; Right, bright-spot area vs. time of the same particle, showing very similar characteristics

Due to the difficulty of setting the right optical conditions to remain within the pixel value limits while still capturing the remaining combustion events, the bright-spot area vs. time plots will be used in lieu. However, the very close resemblance between pixel value and bright-spot area implies that the bright-spot areas are correlated with the particle temperature since the light intensity can be correlated to temperature by the Stefan-Boltzmann law:

$$q = \sigma T^4 A \tag{21}$$

Where q is the radiative heat transfer for a black body, σ is the Stefan-Boltzmann constant, A is surface area, and T is temperature. Although the particles used in the experiment are not black bodies, the relationship is used to justify the assumption that a larger light intensity is qualitatively correlated to higher particle temperature. Figure 11 shows a rare instance of a particle's unsaturated light intensity and area plots vs. time as further evidence of the close correlation between the two

measures. Further, the use of bright-spot against time has been shown to portray characteristics of aluminum particle combustion in a paper by Feng [16].

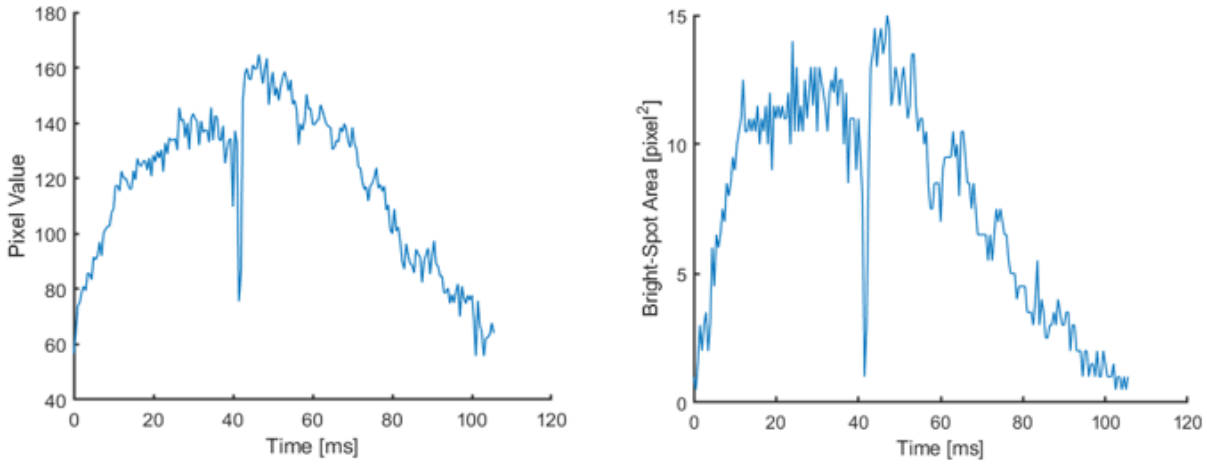

Figure 11: Light intensity vs. time (Left) and bright-spot area vs. time (right) of the same particle. A correlation between the two measurements can be clearly observed. The sudden drop at 40ms is likely due to the thermocouple obscuring measurements.

All results will be presented using bright-spot graphs since it shows a complete picture of combustion characteristics at all optical conditions and is not restricted by a maximum value, unlike light intensity.

The actual value of the bright-spot area is not of interest since the optical conditions change between atmospheres and would thus affect those measurements. Instead, the qualitative trends and shape of the plot are of interest. Therefore, the graphs presented in chapter 4 will be normalized and analysed relatively. The lack of a complete data set due to the COVID-19 pandemic makes the determination of a quantitative value beyond statistical uncertainty very difficult to claim. This is more fully explored in section 4.4, error analysis.

4. Results and Analysis

Chapter 4 contains the results of the experiments carried out prior to the COVID-19 outbreak. Unfortunately, the laboratory shut down before data could be collected for the xenon gas mixtures and for a different particle size. Furthermore, the dataset for the 60% helium – 40% oxygen gas mixture was particularly small.

Each experimental set of data is compared against two theoretical approximations of the combustion:

- The regime-dependent combustion time model explored in section 2.1.3, which assumes all combustion events occur in the same combustion regime. Equations (8) and (9) give the combustion time in the kinetic and diffusive regimes respectively.
- The second theory is the time-dependent combustion analysis discussed in section 2.1.4, which accounts for changes in particle size and combustion regime over time. Equations (13) and (14) form a set of differential equations that can be solved using a MATLAB program as shown in [8].

The properties and ratios used in the theoretical calculations of iron combustion in different atmospheres are listed in Table 1.

Table 1: List of properties and ratios used for theoretical calculations

Gas Mixture	λ Thermal Conductivity W/mK	c_0 Spec. Heat Capacity $[J/kgK]$	ρ_0 Gas Mass Density $[kg/m^3]$	i Stoichio-metric Index	C_0 Oxidizer Mass Concentration $[kg/m^3]$	q Heat of Reaction $[J/kg]$	$m_{0,\infty}$ Mass Fraction of Oxygen
21O-He	0.2095	2285	0.411	2.8	0.105	8.94 e6	0.680
40O-He	0.1707	1593	0.632	2.36	0.210	8.94e6	0.842
21O-Ar	0.03427	590	1.595	2.8	0.105	8.94 e6	0.176
40O-Ar	0.0376	658	1.529	2.36	0.210	7.38e6	0.348
Air (21O-Ni)	0.0457	1000	1.205	2.8	0.105	8.94 e6	0.235

Thermal conductivity was approximated by multiplying each individual gas' thermal conductivity by their molar fraction since it is largely dependent on the collision between atoms to transfer energy [17]. Further, the stoichiometric index was obtained by assuming that combustion in 40% oxygen-argon atmosphere resulted in a majority of Fe_2O_3 oxides whereas combustion in the 21% oxygen atmospheres resulted primarily in Fe_3O_4 and FeO oxides [6, 18].

The pre-exponential factor represents the frequency of collision between reactant molecules. It was approximated building off the values used in modelling the combustion of single aluminum particles by Friedman and Maček [19], and adjusting for the difference in gas temperatures. Both cases consider gaseous oxygen's collision with the surface of a solid metal particle and thus it is assumed that the only change in the mechanics of the collision is the gas' temperature. After scaling for the temperature, the pre-exponential factor was determined to be 43m/s. The value for the activation energy was based on the findings of Grosvenor, Kobe, and McIntyre which calculated the activation energy of the oxidation of iron by oxygen gas to be 32kJ/mol [20].

By inputting the parameters in equations (8) and (9), the kinetic and diffusive combustion times were calculated respectively. The results are presented in Table 2.

Table 2: Combustion times from the regime-dependent combustion time model

Gas Mixture	Kinetic [ms]	Diffusive [ms]
21%O – 79%He	125.4	2.578
40%O – 60%He	78.10	2.149
21%O – 79%Ar	124.8	10.83
40%O – 60%Ar	78.11	7.354
Air (21%O – 78%Ni)	123.7	10.90

The kinetic burning times in Table 2 clearly show a strong dependence on the molar concentration of oxygen while changing the pairing gas makes virtually no difference. This is because the higher density when comparing argon to helium is offset by the lower specific heat capacity. Combustion time in the diffusive regime shows an inverse correlation with the diffusivity of the gas mixture, which is proportional to the thermal diffusivity based on the assumptions made in this section.

The large difference in combustion times between the two combustion regimes for the same particle size and gas mixtures indicate the possibility of cases where the combustion event occurs in a mixed or intermediate combustion regime. These cases would have combustion times within the bounds of the purely kinetic and diffusive combustion times in Table 2. These nuances are better captured by the time-dependent combustion model which are presented alongside the experimental results in the subsequent sections.

4.1 Helium – Oxygen Mixtures

4.1.1 21% Oxygen – 79% Helium

This gas mixture was very difficult to capture on camera since most particles would not ignite. Because there were few observable combustion events at the usual pre-heater temperature of 750K, the temperature was exceptionally brought up to 940K. In addition, the optical condition on the camera allowed for the most light of all experiments conducted: aperture was set to 32 and no filters were used.

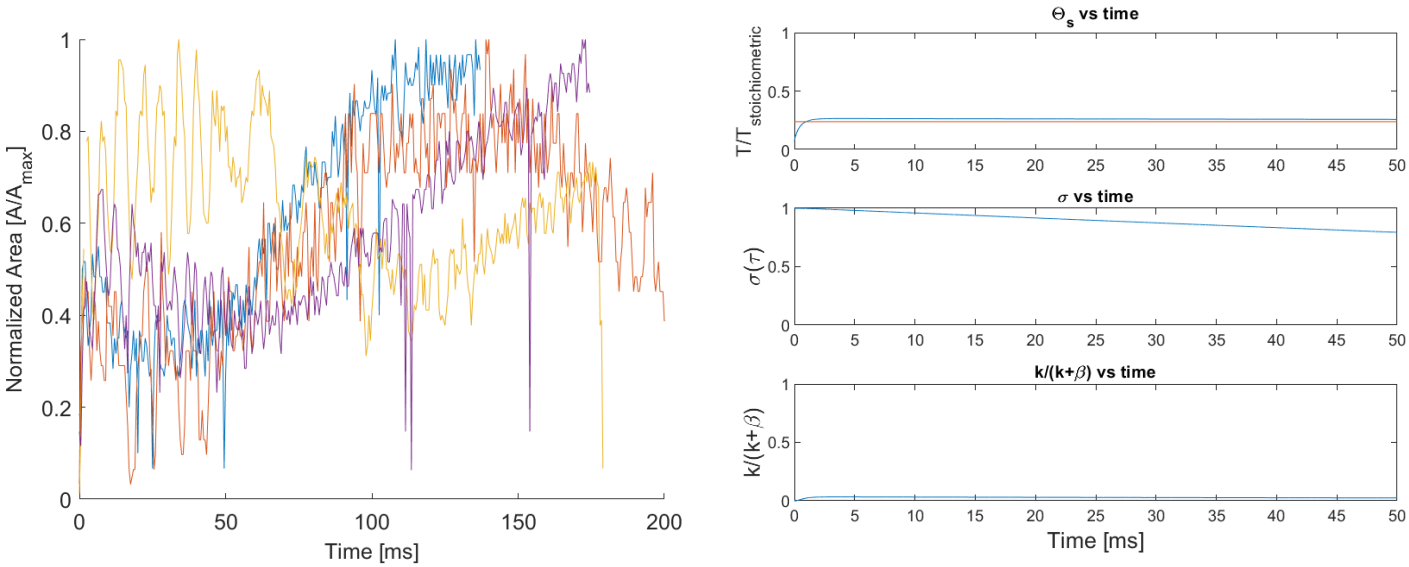

Figure 12: Left: Normalized area vs. time in 21% oxygen – 79% helium, each colour represents a particle. Right: Time-dependent combustion model results for 21% oxygen – 79% helium, profiles of particle temperature, radius, and normalized Damköhler number over time.

The experimental data in Figure 12 shows no discernable trend in the plot and shows very large fluctuations in the data for every particle. This is because overall, the bright-spot area of the particles mostly remained constant and thus minor fluctuations result in major fluctuations in the normalized area. The theoretical model shows the particle increase in temperature, reaching the

ambient gas temperature which is characteristic of a highly kinetic regime. The theoretical plot shows the Damköhler number staying close to 0 throughout, confirming a kinetically limited combustion which explains the lack of trend in Figure 12 since the particle does not experience ignition.

4.1.2 40% Oxygen – 60% Helium

As mentioned at the start of this chapter, very little data was collected for this gas mixture. The optical conditions used were an aperture of 11 and a 10x optical filter.

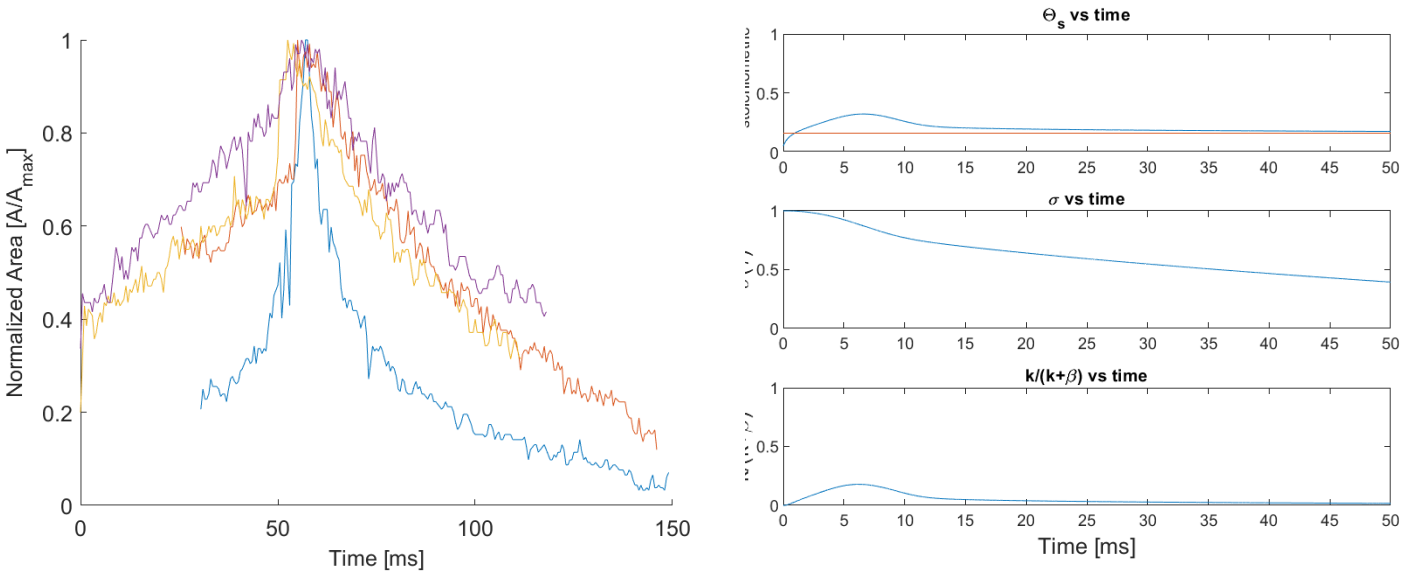

Figure 13: Left: Normalized area vs. time in 40% oxygen – 60% helium, each colour represents a particle. Right: Time-dependent combustion model results for 40% oxygen – 60% helium, profiles of particle temperature, radius, and normalized Damköhler number over time.

Although the experimental data in

Figure 13 differs wildly between particles, the underlying trend is of a swelling in the normalized area, which was not observed in the 21% oxygen – 79% helium mixture. The theory shows a

similar trend albeit on a much smaller timescale, indicating that the combustion regime was briefly in a transitional state. Unfortunately, no further conclusions can be made because of the small sample size.

4.2 Argon – Oxygen Mixtures

4.2.1 21% Oxygen – 79% Argon

This gas mixture was filmed using an aperture of 8 and a 10x optical filter.

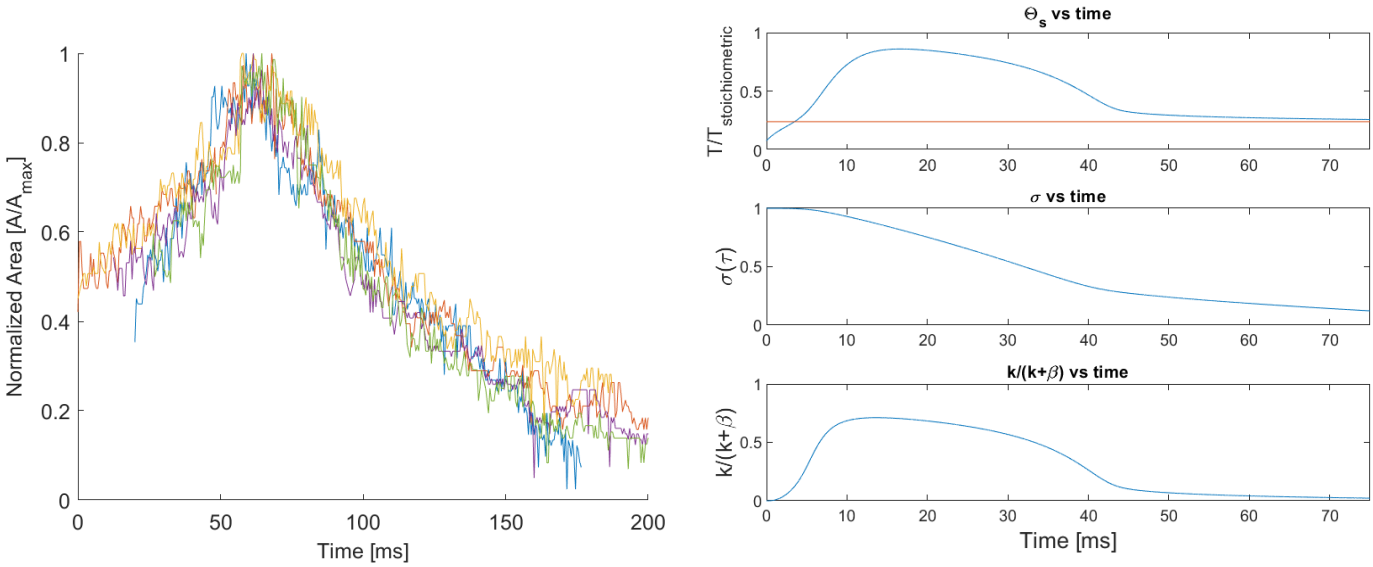

Figure 14: Left: Normalized area vs. time in 21% oxygen – 79% argon, each colour represents a particle. Right: Time-dependent combustion model results for 21% oxygen – 79% argon, profiles of particle temperature, radius, and normalized Damköhler number over time.

The experimental results for the gas mixture shown in Figure 14 has a very evident trend among all the particles plotted. A gradual increase in the normalized bright-spot area up to unity, followed by a gradual decrease can be observed over the course of the combustion event. The theoretical plot on the left shows the particle reaching a Damköhler number above 0.5 indicating a shift

towards the diffusive regime for around 35ms. During that span, the normalized temperature also reaches a high plateau while the rate of change in the radius, and thus mass consumption, is more rapid. The Damköhler number then falls back to near-zero indicating a return to the kinetic regime, while the normalized temperature and rate of change of radius subside. In Figure 14, the theoretical model seems to correctly anticipate the width and intensity of the peak displayed in the experimental data.

4.2.2 40% Oxygen – 60% Argon

Camera conditions were the most light-restrictive in this gas mixture as the combustion events were the most vigorous of the experiments. The aperture was set to 16 in addition to a 10x filter.

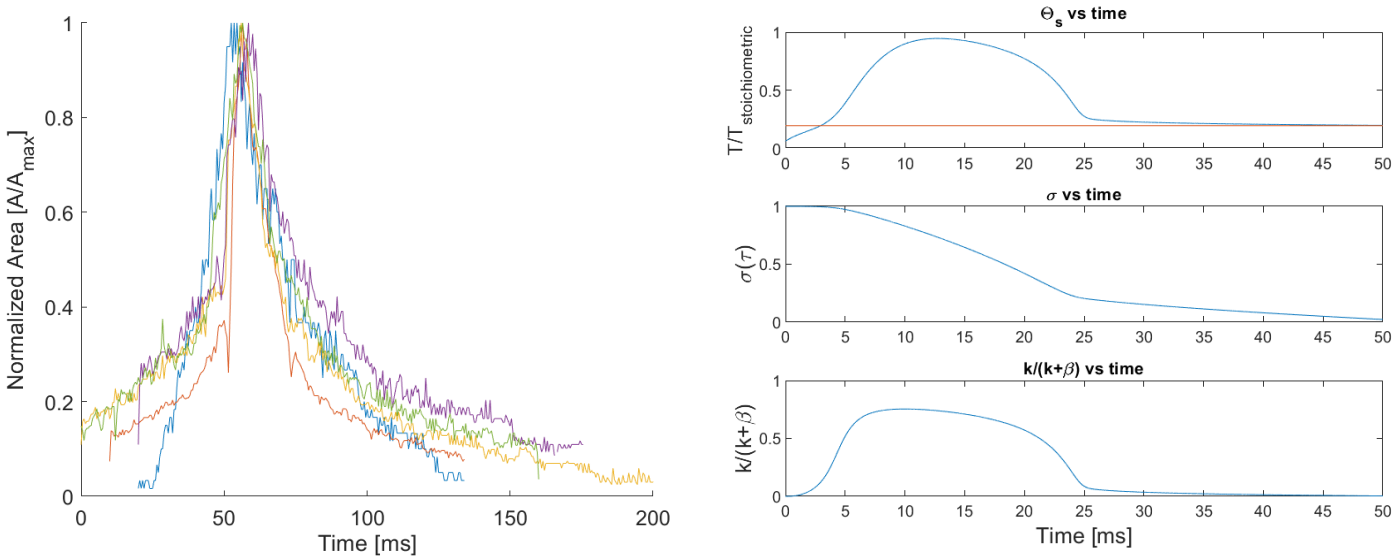

Figure 15: Left: Normalized area vs. time in 40% oxygen – 60% argon, each colour represents a particle. Right: Time-dependent combustion model results for 40% oxygen – 60% argon, profiles of particle temperature, radius, and normalized Damköhler number over time.

The experimental results in Figure 15 show a very abrupt peak for all the different particles. The theoretical plots have a rise in the Damköhler number spanning around 22ms, which is roughly the

width of the peaks in the experimental data. Since the bright-spot area is correlated with particle temperature as mentioned in chapter 3, the theoretical and experimental data matches very well for this gas mixture. The transition from the kinetic regime towards a more diffusive regime, shown by the normalized Damköhler number reaching around 0.75, produces the sharp peak, where temperature and rate of change in radius reach their highest values. This is followed by a rapid drop back to the kinetic regime as the radius shrinks below a critical size as shown in the theoretical data and validated by the experimental observations. As with the 21% oxygen – 79% argon mixture, the time-dependent combustion model correctly predicted the combustion behaviours of the particle in this gas mixture.

4.3 Nitrogen – Oxygen Mixture (Air)

4.3.1 21% Oxygen – 78% Nitrogen

Due to the low amount of data collected, the set of data used for tests and calibration was analysed. To film the combustion events in air, an aperture of 8 was used with a 10x optical filter. Theoretically, the properties of air (nitrogen-oxygen) display many similarities with the argon-oxygen mixtures as shown by their properties in Table 1Table 2. These similarities are further displayed in Figure 16, showing similar combustion profiles experimentally and theoretically with the 21% oxygen -79% argon results in Figure 14.

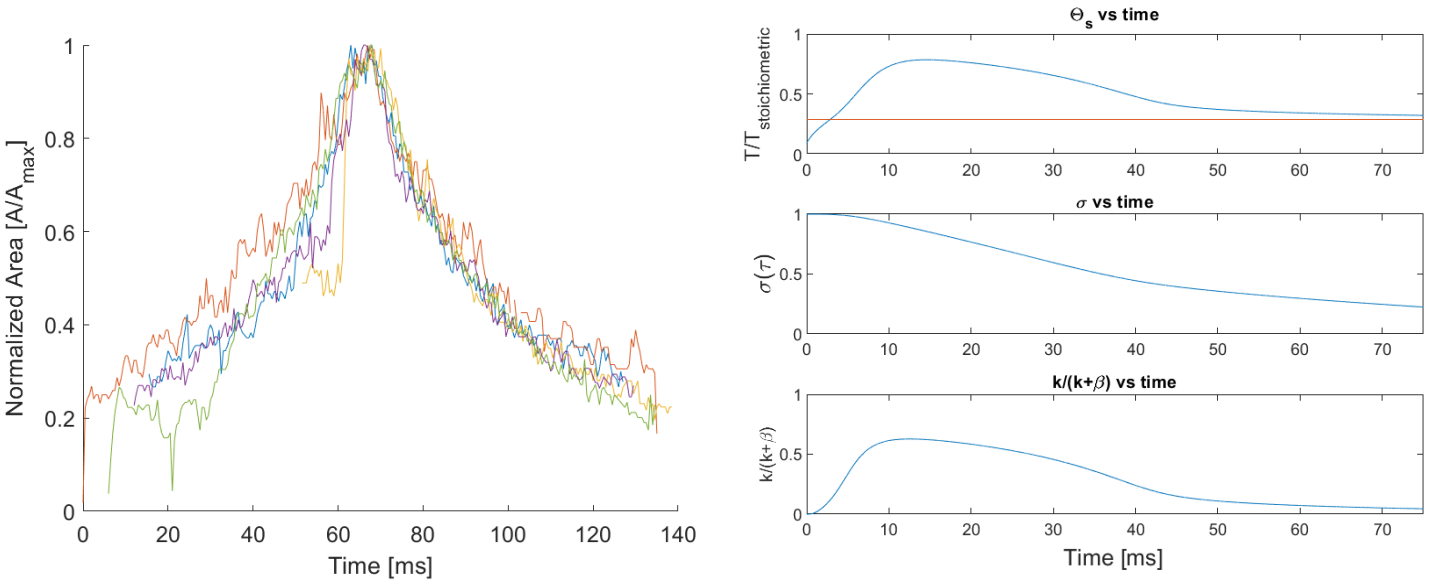

Figure 16: Left: Normalized area vs. time in 21% oxygen – 78% nitrogen, each colour represents a particle. Time-dependent combustion model results for21% oxygen – 78% nitrogen, profiles of particle temperature, radius, and normalized Damköhler number over time.

As was the case with Figure 14, the results shown in Figure 16 display a gradual climb to a peak value of normalized area followed by a gradual decline, with the theoretical data accurately predicting the width of the peak. The time-dependent model shows the normalized Damköhler number approach and sustain a value around 0.5 for approximately 35ms, indicating a combustion occurring in an intermediate regime. This is well contrasted by the theoretical results in the 40% oxygen – 60% argon mixture, where the normalized Damköhler number approaches 0.75 indicating a more-diffusive regime, and shown experimentally by the sharper peak in Figure 15.

4.4 Sources of Error

The initial objective of this thesis was to film a sufficient number of combustion events in the selected atmospheres to ultimately create a set of histograms describing the frequency of different

burn times. This would then be used to determine an average combustion time value for each particle size-atmosphere combination. However, after surveying the amount of data collected before the experiments were cut short by the COVID-19 outbreak, it was determined that determining a quantitative property such as the burning times of iron particles would be too prone to variation due to insufficient data points collected. To illustrate the point, the standard deviation for a normal distribution is given as

$$\sigma = \sqrt{\frac{1}{\mathrm{N}} \sum_{i=1}^{N} (x_i - \mu)^2} \tag{22}$$

Where x is a specific data point, μ is the mean, and N is the sample size. The standard deviation from the mean is inversely related to the sample size meaning that due to the small number of samples collected, the variability would have high chances of being unreasonably large such that the determined combustion times would be statistically meaningless. The significance levels and p-values are not considered in this statistical analysis since the objective was to determine a combustion time distribution for a given particle size and gas mixture, not test a hypothesis. For this reason, the decision was made to compare the data on a qualitative basis, changing the objective from obtaining combustion time values to focusing more on the observable characteristics of iron particle combustion in the different gas mixtures.

Other identified sources of error are listed in this section:

- The glare of the burning particles in the quartz tube posed a risk for error as it would be recorded by the camera and processed by the MATLAB program, potentially doubling a

data point for one particle. To mitigate this error source, the results from the MATLAB program were analysed against the videos to only select the plots representing the particles, while filtering out the glare. Although effective, this method is time-consuming.

- The MATLAB program discretizes each video into their component frames which presents a source of error. However, the high-speed camera films at 2000 frames per second and thus the time elapsed between frames is 0.5 milliseconds, which is at least two orders of magnitude below the timescales used in the qualitative analysis but would have been significant in determining combustion times. The MATLAB program also binarizes each image using a pixel threshold value. A higher value leads to less noise produced by reflections but may not capture the tail ends of a combustion event. A lower value captures more events but creates more noise making the particle-tracking more challenging. Ultimately, this error was not a problem as all values were normalized in the qualitative analysis and the interest was in the shape of the combustion profiles as opposed to specific numerical data.
- Different optical conditions were used for filming the combustion events in the different gas mixtures to avoid oversaturation. This changes the amount of light captured by the camera which would in turn change the quantitative data obtained from the frames. However, the decision to analyse qualitatively shifted the focus of the thesis away from the numerical data obtained, effectively nullifying this error source through normalization of data.
- The particles were injected into the apparatus by lightly tapping a syringe. These taps create a potential for error by varying the velocity of the injected particles. Similar to the previous

sources of errors, this error is not relevant in the context of a qualitative analysis but would have been significant in any quantitative analysis.

5. Discussion

5.1 Data-Theory Comparison

As stated in the previous chapters, this thesis was restricted to qualitative analyses due to the COVID-19 pandemic. Nonetheless, a notable correlation between the width of the peaks in the normalized bight-spot area found experimentally, and the time-dependent combustion model's results is apparent. The argon-oxygen and nitrogen-oxygen (air) gas mixtures had normalized-area peaks spanning the same amount of time as their theoretical normalized Damköhler numbers had values around 0.5-0.8, indicating a mixed combustion regime. The 21% oxygen-79% helium mixture showed no discernible trend in the experimental data, which agrees with the time-dependent combustion model showing a nearly pure kinetically-limited combustion. Furthermore, the increase of the preheater temperature by around 200K, increased the frequency of combustion events, showing a correlation with the ambient gas temperature: a characteristic of kinetically-limited combustion. The 40% oxygen – 60% helium results were unfortunately inconclusive because of the lack of data. From those observations, it appears the time-diffusive combustion model approximates the experimental combustion events accurately.

Apart from the 21% oxygen – 79% helium mixture, all other theoretical models had their normalized Damköhler numbers plateau temporarily to an intermediate value implying that the combustion event occurred between the fully kinetic and diffusive regimes. This is further supported by the fact that the combustion times in the time-dependent model are within the bounds set by the kinetic and diffusive combustion times calculated using the regime-dependent model, for all gas mixtures.

Unfortunately, determining a combustion time experimentally is not possible without adequate quantitative information. As shown in the results, the combustion regime of the particle over time transitions from an intermediate or more-diffusive regime towards the kinetic regime, effectively creating two contrasting types of combustion behaviours. The difficulty lies in determining where the kinetic burning of the particle ends, and the cooling of the particle begins. This could be done if an optical spectrometer was used to determine the light emission, which could be related to temperature using the Stefan-Boltzmann law. The rate of change of the particle temperature could then be compared against the approximated cooling rate of the particle to distinguish a kinetic combustion from natural cooling of the particle.

5.2 Effects of Atmospheres

The main variables in this experiment were the gas mixtures composed of argon, helium, or nitrogen, paired with different concentrations of oxygen.

By comparing the experimental and theoretical results for the argon-oxygen gas mixtures to the helium-oxygen gas mixtures, the effects of the gas' transport properties becomes apparent. The mass diffusivity and thermal conductivities of gases are proportional to each other. In turn, these two properties are proportional to the gas' average molecular speed which is inversely correlated to the molecular mass of the gas. Therefore, replacing argon gas with helium, a much lighter gas, greatly increased the thermal conductivity of the oxidiser as detailed in Table 1. The physical consequence of this change is that the helium gas mixtures, with their higher thermal conductivity, more easily cools the particle as shown in Figure 17.

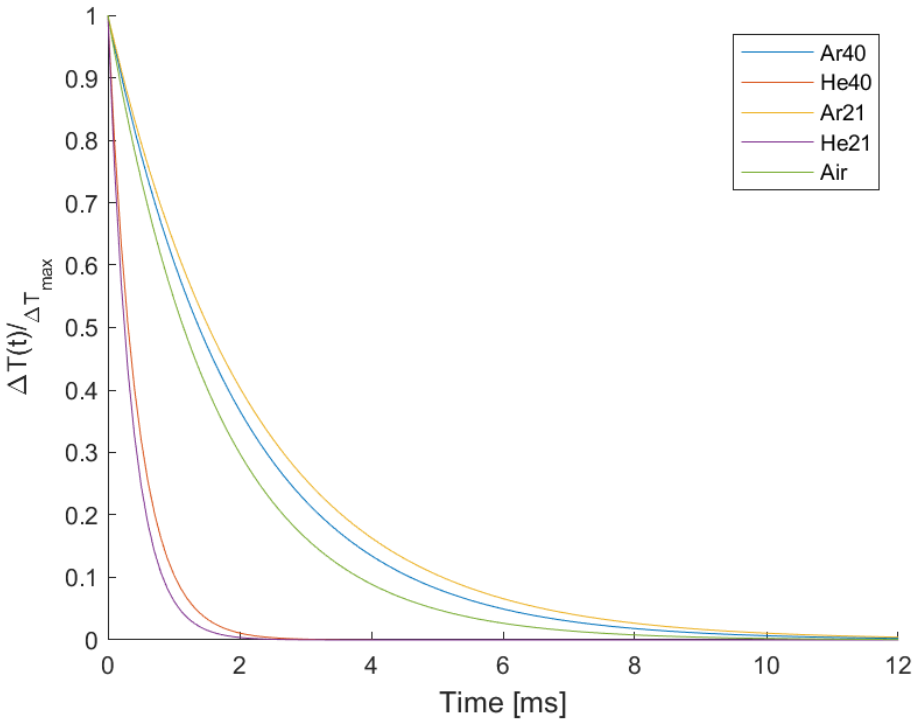

Figure 17: Normalized cooling curve for the different gas mixtures. Mixtures are labelled as the non-oxygen gas element, followed by the oxygen concentration by molar fraction.

The curves in Figure 17 were calculated using equation (20), restated here for simplicity.

$$\frac{T(t) - T_\infty}{T_i - T_\infty} = exp\left(\frac{-3\mathrm{h}t}{r\rho C_p}\right) \tag{20}$$

Where $h = \frac{Nu\lambda}{2r_p} = \frac{\lambda}{r_p}$, where the Nusselt number is obtained from the Ranz-Marshall correlation which can be expressed as,

$$Nu = 2 + 0.6Re^{(1/2)}Pr^{(1/3)} \approx 2 \tag{23}$$

Since the Reynold number is very small due to the particle size and low velocities. The different cooling rates shown in Figure 17 explain why the argon gas mixtures reached higher normalized Damköhler numbers and temperatures in the time-dependent model, and were experimentally seen

to show sharper peaks in normalized bright-spot area when compared to the helium gas mixtures of the same oxygen concentration. This is because a higher mass diffusivity would lead to a larger diffusive term, $\beta = D/r$, in the normalized Damköhler numbers, $Da^* = \frac{k}{k+\beta}$, causing the value to move towards 0, which represents the kinetically-limited regime.

The impact of varying the oxygen concentration within the same oxidizer pair is observed to influence the intensity of the light emitted during the combustion event. Experimentally, the 40% oxygen gas mixtures always required optical conditions that were more restrictive to light, indicating a brighter combustion event. Since area was assumed to be correlated to light intensity which is related to temperature using the Stefan-Boltzmann law, it can be experimentally shown that the higher oxygen fractions lead to higher combustion temperature. This is theoretically supported by equation (16) restate here,

$$T_s = T_0 + (Da^*)\frac{qiC_0}{c_0\rho_0} \tag{16}$$

showing the dependence of the particle surface temperature on the oxidizer mass concentration, C_0 in diffusively-limited combustion. The variable T_g is the gas temperature, q is the heat of reaction, i is the stoichiometric ratio, ρ_0 is the gas density, and c_0 is the gas heat capacity. Furthermore, a larger concentration of oxygen was seen to reduce the time of combustion because the rate of reaction is dependent on the rate of collisions of oxygen with the particle surface. As the oxygen concentration is increased, the rate of reaction increases, causing a more vigorous combustion which lasts a shorter amount of time.

An interesting note is that the product of the gas density and heat capacity for the helium-oxygen and argon-oxygen gas mixtures are approximately the same, meaning that for a given oxygen molar fraction, the theoretical stoichiometric flame temperature would be near identical. In other words, equation (16) for the two gas mixtures would be identical, with the exception of the Damköhler number. Experimentally, the argon and helium mixtures with 40% oxygen were the two gas mixtures requiring the highest levels of light restrictions when filming; however, the argon mixture needed a higher aperture compared to the helium mixture, indicating higher a higher temperature combustion. This is proof that the argon-oxygen mixture is burning in a more diffusive regime than the helium-oxygen mixtures since their surface temperature would only differ in the magnitude of the Damköhler number [21].

6. Conclusion

6.1 Conclusion

This experimental thesis work showed the greater theoretical accuracy and value of the time-dependent combustion model, which takes the intermediate cases of combustion regimes into account in contrast with the regime-dependent models. Theoretically, the time-dependent model predicted combustion times that were consistently between the purely diffusive and kinetic time calculations, which was in accord with the experimental values collected. The time-dependent model was also able to accurately predict the timespan of the normalized bright-spot area profile peaks, demonstrating the model's ability to account for the dynamic transitions between the combustion regimes.

Determining actual combustion times proved to be difficult in this context because of the challenge in discerning the natural cooling of the particle from the kinetic burning without quantitative values. A more complete and quantitative set of results could have been obtained had time not been cut short by the COVID-19 outbreak, and with the use of additional equipment such as an optical spectrometer.

It was observed that particles the helium - oxygen gas mixtures had considerable difficulty igniting, which was supported by the time-dependent model indicating a mostly kinetic combustion regime for the gas mixtures. In contrast, particles in the argon - oxygen gas mixtures were observed to burn much more readily and brighter, indicating that the combustion event was closer to its adiabatic flame temperature and thus in a more diffusive regime compared to the helium mixtures of equivalent oxygen concentrations. This observation was theoretically corroborated by the time-

dependent model. Increasing the oxygen fraction in the gas was observed to increase the intensity and brightness of the combustion event, while decreasing the combustion time. Theoretically, it was shown that a higher oxygen fraction increases the stoichiometric flame temperature, and that helium and argon have similar flame temperatures for the same oxygen fraction. Despite this, there was an experimental difference in brightness when comparing oxygen-argon and oxygen-helium mixtures with the same oxygen mole fraction. This was seen as proof that the particle combustion in the oxygen-helium oxidizers burn in a more kinetically-limited regime when compared to the oxygen-argon mixtures of the same oxygen concentrations.

Despite the major disturbance caused by the laboratory shutdown, this thesis work shows the importance of the k-beta model in the context of studying the combustion of metal powders, especially for use as metal fuels. It also developed an experimental apparatus and post-processing MATLAB program which should substantially increase the speed of further analyses on this topic. Suggestions for future work on this topic are mentioned in the next section.

6.2 Future Work

Future work and potential improvements to the experimental design are listed here:

- Use of an optical spectrometer: this would allow for quantitative results of the combustion events allowing for a more concrete analysis relative theory and literature. The use of a spectrometer to capture the full range of the light intensity versus time would allow for a direct comparison with temperature instead of using the particle bright-spot area as an intermediary.

- Adding a cylindrical ceramic heater at the base of the apparatus. Doing so would allow the gas to be heater at a much higher temperature than is currently the case. This increase would make the combustion events more reliably occur in the experimental section. Further, it would allow for variation in the gas temperature, making it another parameter that could be studied. The current half-cylindrical can only reach temperature of around 850K whereas the cylindrical heaters have demonstrated their ability to reach temperatures up to 1250K. The bending of the quartz tube has been a problem in the experiments conducted, but the phenomenon is hypothesised to be due to the uneven heat-distribution in the semi-cylindrical heater causing the tube to buckle under its weight toward the hotter section. Therefore, adding a heater with even heat-distribution should not exacerbate the problem
- Obtain velocity measurements. Adding the velocity of the particle to the set of data collected could be of use in calculating heat transfer characteristics and would help account for errors caused by varying injection speeds. This could be done by filming a ruler alongside the videos to determine the pixel-to-distance ratio which the post-processing MATLAB function could use to calculate the velocity.
- Improving the injection mechanism. As mentioned in the error analysis section, a more sophisticated injection mechanism would reduce the errors caused by the varying injection speeds. However, this is a challenging improvement due to the difficulty of designing for the extremely small particles used for these experiments.

References

[1] H. Ritchie and M. Roser. (2020). *Energy*.

[2] BP, "Statistical Review of World Energy " 2019.

[3] J. M. Bergthorson *et al.*, "Direct combustion of recyclable metal fuels for zero-carbon heat and power," *Applied Energy,* vol. 160, pp. 368-382, 2015/12/15/ 2015.

[4] J. M. Bergthorson, "Recyclable metal fuels for clean and compact zero-carbon power," *Progress in Energy and Combustion Science,* vol. 68, pp. 169-196, 2018/09/01/ 2018.

[5] H. Ritchie and M. Roser. (2020). *CO2 and Greenhouse Gas Emissions*.

[6] F. D. Tang, S. Goroshin, A. Higgins, and J. Lee, "Flame propagation and quenching in iron dust clouds," *Proceedings of the Combustion Institute,* Article vol. 32 II, pp. 1905-1912, 2009.

[7] A. Wright, S. Goroshin, and A. J. Higgins, "Combustion Time and Ignition Temperature of Iron Particles in Different Oxidizing Environments " presented at the International Colloquium on the Dynamics of Explosions and Reactive Systems, Leeds, UK, 2015.

[8] M. Soo, X. Mi, S. Goroshin, A. J. Higgins, and J. M. Bergthorson, "Combustion of particles, agglomerates, and suspensions – A basic thermophysical analysis," *Combustion and Flame,* vol. 192, pp. 384-400, 2018/06/01/ 2018.

[9] K. Keishi, "Flames in Non-volatile Reactive Particle Suspensions," Undergraduate Honours Program, Department of Mechanical Engineering, McGill University Montreal, 2015.

[10] S. Goroshin, F.-D. Tang, A. J. Higgins, and J. H. S. Lee, "Laminar dust flames in a reduced-gravity environment," *Acta Astronautica,* vol. 68, no. 7, pp. 656-666, 2011/04/01/ 2011.

[11] F.-D. Tang, S. Goroshin, and A. J. Higgins, "Modes of particle combustion in iron dust flames," *Proceedings of the Combustion Institute,* vol. 33, no. 2, pp. 1975-1982, 2011/01/01/ 2011.

[12] M. J. Soo, K. Kumashiro, S. Goroshin, D. L. Frost, and J. M. Bergthorson, "Thermal structure and burning velocity of flames in non-volatile fuel suspensions," *Proceedings of the Combustion Institute,* vol. 36, no. 2, pp. 2351-2358, 2017/01/01/ 2017.

[13] M. Soo, S. Goroshin, J. M. Bergthorson, and D. L. Frost, "Reaction of a Particle Suspension in a Rapidly-Heated Oxidizing Gas," vol. 40, no. 4, pp. 604-612, 2015.

[14] R. Yetter and F. Dryer, *Metal Particle Combustion and Classification*. Cleveland, OH, USA: Academic Press, 2001.

[15] G. G. Stokes, "Transactions of the Cambridge Philosophical Society: Part X. *On the Effect of the Internal Friction of Fluids on the Motion of Pendulums*," 1822.

[16] Y. Feng, Z. Xia, L. Huang, and L. Ma, "Ignition and combustion of a single aluminum particle in hot gas flow," *Combustion and Flame*, vol. 196, pp. 35-44, 2018/10/01/ 2018.

[17] E. A. Mason, "Gas: Thermal Conductivity " *Encyclopaedia Britannica* 2020.

[18] J. Palečka, J. Sniatowsky, S. Goroshin, A. J. Higgins, and J. M. Bergthorson, "A new kind of flame: Observation of the discrete flame propagation regime in iron particle suspensions in microgravity," *Combustion and Flame*, vol. 209, pp. 180-186, 2019/11/01/ 2019.

[19] R. Friedman and A. Maček, "Ignition and combustion of aluminium particles in hot ambient gases," *Combustion and Flame*, vol. 6, pp. 9-19, 1962/01/01/ 1962.

[20] A. P. Grosvenor, B. A. Kobe, and N. S. McIntyre, "Activation energies for the oxidation of iron by oxygen gas and water vapour," *Surface Science*, vol. 574, no. 2, pp. 317-321, 2005/01/10/ 2005.

[21] M. McRae, P. Julien, S. Salvo, S. Goroshin, D. L. Frost, and J. M. Bergthorson, "Stabilized, flat iron flames on a hot counterflow burner," *Proceedings of the Combustion Institute*, vol. 37, no. 3, pp. 3185-3191, 2019/01/01/ 2019.